Journal of Power Sources 273 (2015) 1127–1135

Contents lists available at ScienceDirect

Journal of Power Sources

journal homepage: www.elsevier.com/locate/jpowsour

Improved performance of lithium ion battery separator enabled by co-electrospinnig polyimide/poly(vinylidene fluoride-co-hexafluoropropylene) and the incorporation of TiO_2-(2-hydroxyethyl methacrylate)

Weiya Chen [a], Yanbo Liu [a, b, *], Ying Ma [a], Wenxiu Yang [a]

[a] School of Textiles, Tianjin Polytechnic University, Tianjin 300387, China
[b] Key Laboratory of Advanced Textile Composites of Ministry of Education, Tianjin 300387, China

HIGHLIGHTS

- TiO_2-HEMA was prepared by atom transfer radical polymerization.
- Nanoparticles@PI/PVdF-HFP membranes were prepared by co-electrospinning process.
- TiO_2-HEMA@PI/PVdF-HFP membrane thermally treated has the highest tensile strength.
- The addition of TiO_2-HEMA improves the electrochemical properties of membranes.

GRAPHICAL ABSTRACT

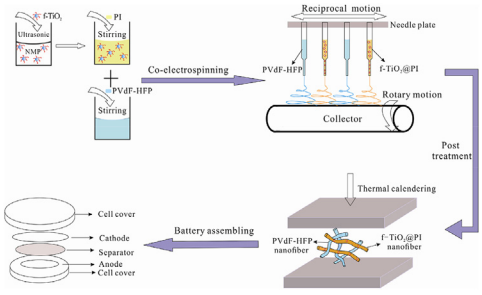

ARTICLE INFO

Article history:
Received 12 July 2014
Received in revised form
3 October 2014
Accepted 4 October 2014
Available online 13 October 2014

Keywords:
Co-electrospinning
Separator
Lithium ion battery
2-Hydroxyethyl methacrylate grafted TiO_2
Thermal calendering

ABSTRACT

Functionalized TiO_2 (f-TiO_2) was synthesized by the atom transfer radical polymerization process and then three types of composite nanofiber membranes including PI/PVdF-HFP (PI/PH, with no nanoparticles contained in PI), TiO_2@PI/PVdF-HFP (T@PI/PH, with TiO_2 mixed in PI) and f-TiO_2@PI/PVdF-HFP (f-T@PI/PH, with f-TiO_2 blended in PI) were prepared by bicomponent co-electrospinning technique which could separately maintain the original properties of both PVdF-HFP and PI nanofibers. UV–vis characterization manifested that the modified nanoparticles can provide significant improvements in reducing the particle agglomeration. Morphology, porosity, electrolyte uptake and liquid electrolyte contact angle of all the electrospun separators were investigated, and results showed that the composite separator with 2% f-TiO_2 nanoparticle had smaller fiber diameter, higher porosity, larger electrolyte uptake, smaller contact angle and more excellent thermal dimensional stability. More importantly, the tensile strength of all the composite membranes increased by more than three times after thermal calendering process, which resulted from the several bonded points caused by the fusion of PVdF-HFP component with low melting temperature. Additionally, electrochemical properties of PI/PH, 2% T@PI/PH and 2% f-T@PI/PH composite separators and cycling performances of corresponding batteries were evaluated and 2% f-T@PI/PH composite separator showed better properties than the other two.

* Corresponding author. School of Textiles, Tianjin Polytechnic University, Tianjin 300387, China. Tel.: +86 22 83955353; fax: +86 22 83955287.
E-mail address: yanboliu@gmail.com (Y. Liu).

http://dx.doi.org/10.1016/j.jpowsour.2014.10.026
0378-7753/

1. Introduction

Lithium-ion battery serving as one kind of rechargeable energy sources has been widely applied in portable electronic devices, plug-in hybrid electric vehicles (PHEVs) and energy storage systems [1,2]. A lithium-ion battery is comprised of four components including cathode, anode, liquid electrolyte and separator, where the separator acts as a physical barrier between the cathode and the anode to avoid the occurrence of short circuit due to the direct contact, and meanwhile sustains the liquid electrolyte facilitating lithium ions to transport rapidly. Nowadays, microporous membranes such as polypropylene (PP), polyethylene (PE) and PP/PE/PP composite separators are commercially used in lithium-ion battery due to their superior chemical stability, significant mechanical property and thermal shut-down performance [3–5]. However, these polyolefin-based separators possess inherent hydrophobicity and lower porosity, resulting in poor wettability and liquid electrolyte uptake, and thus the low ionic conductivity and poor capacity of the battery. In addition, the poor thermal stability resulting from their relatively low softening or melting temperatures may make the battery assembled with polyolefin based separator more susceptible to explosion at higher temperature conditions when the internal electric short circuit occurs [6–9].

Recently, electrospinning technology has been extensively investigated in order to obtain multi-microporous nanofiber membranes with high porosity for applications in battery separators [10–12], and inorganic nanoparticles have been used as modification additives to enhance the performance of the resulting nanofiber-based separator. Wu et al. [12] prepared electrospun TPU/PVdF blending membrane with 3% in situ TiO_2, and 9% solution of TPU/PVdF in DMF/acetone. The resultant nanoparticle modified electrospun separator showed increased ionic conductivity, electrochemical stability and mechanical property. However, although this method could efficiently improve the foresaid performance by blending electrospun TPU/PVdF with in situ TiO_2, the optimal mechanical property and thermal shutdown feature could not be achieved by blending the two polymers in one solution system, because this polymer blending method tends to mix the two polymers at molecular level and generate/create a new type of mono-component polymer based nanofiber web, which combines the characteristics of the both polymers, incapable of separately keeping the individual features of each polymer, no component acting as binder and hence the optimistic mechanical strength and thermal shutdown function could not be attained eventually. Lee et al. [13] prepared nanoparticle modified nanofibrous separator via electrospinning a poly(amic acid) (PAA) solution followed by an imidization process, and then dip-coating thin layer of Al_2O_3 nanoparticles on both sides of the resultant PI electrospun membrane. The resulting separator exhibited enhanced capacity and rate capabilities, with a limited increase of cell impedance. Again, this type of battery separator is actually composed of mono-component polymer and hence incapable of obtaining optimal mechanical property or thermal shutdown function. Another drawback of these methods is that the nanoparticles which served as modification additives are prone to aggregate due to their extremely large specific surface area, providing a tremendous driving force for particle adhesion [14] and hindering the effect on the improvement of battery performance. Based on these considerations, maintaining the original property of the polymers as bonded fiber in composite membranes and modifying the dispersibility of nanoparticles in polymer solution are quite necessary.

As we all know, grafting another polymer on the surface of nanoparticles is an effective way to enhance the dispersity of nanoparticle in polymers, via developing specific interactions between nanoparticles and the polymer [15]. In the present study, PI/PVdF-HFP composite nanofiber separator with the addition of various contents of TiO_2 and functionalized TiO_2 (f-TiO_2) nanoparticles were prepared by a bicomponent co-electrospinning method, which was addressed in our previous research [16]. The f-TiO_2 grafted with 2-hydroxyethyl methacrylate (HEMA) was prepared by atom transfer radical polymerization (ATRP) technique. HEMA has plentiful long polymer chains which can embed into polymer matrix and increase the nanoparticle dispersibility (cf. Fig. 1). The excellent affinity between HEMA and carbonate-based liquid electrolyte and polar surface groups of TiO_2 introducing Lewis acid/based interactions with the ionic species in the liquid electrolyte facilitate the electrospun membrane to entrap more liquid electrolyte and decrease the leakage of the electrolyte [17,18]. Additionally, co-electrospun membrane consists of both the PVdF-HFP and PI nanofibers, with each nanofiber separately keeping its own raw property. Therefore, the tensile strength of composite membranes is expected to be promoted through fusing the PVdF-HFP component, the binding fiber, during thermal calendering process, leading to excellent mechanical property and thermal safety, i.e., the battery is capable of possessing thermal shutdown function due to the existence of PVdF-HFP component having lower melting temperature.

2. Experimental

2.1. Materials and reagents

Poly(vinylidene fluoride-co-hexafluoropropylene) (PVdF-HFP, $M_W = 600{,}000$) and Polyimide (PI, $M_W = 180{,}000$) were provided by Solvay and Dupont, respectively. N,N-Dimethylformamide (DMF), N-methyl-2-Pyrrolidone (NMP), acetone, toluene and methanol in

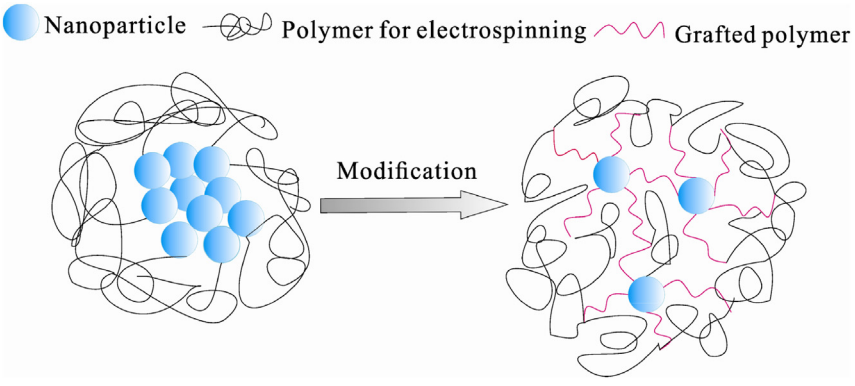

Fig. 1. (a) Agglomerated nanoparticles in the polymer for electrospinning without grafting polymer and (b) separation of particles due to the existence of the grafted polymer.

analytical reagent grade were purchased from Tianjin Weichen Chemical Reagent Co. Ltd. China. Titanium dioxide powder was obtained from Degussa with average particle sizes of 20–30 nm. Triethylamine, 3-aminopropyl triethoxysilane (APTES, 98%), 2-brom-opropionyl bromide (97%), N,N,N′,N″,N‴-pentamethyldiethylenetriamin (PMDETA, 99%), 2-hydroxyethyl methacrylate (HEMA, 96%) and CuBr were supplied by Aladdin Reagent Co., Ltd. (Shanghai, China).

2.2. Synthesis of TiO_2-HEMA

TiO_2 (5 g) nanoparticle was dispersed in 100 ml of toluene and the mixture was stirred for 30 min. Then the mixture was stirred in the nitrogen environment under backflow after 30 ml silane coupling agent was added. At the end of reaction, the product was purified by repeating centrifugal sedimentation (5000 rmp, 5 min) and re-dispersion in toluene for three times aiming at removing excess silane coupling agents. TiO_2–NH_2 was obtained after drying under vacuum for 24 h at 60 °C. The mixture including TiO_2–NH_2 (2 g), toluene (80 ml) and triethylamine (4 ml) was stirred for 40 min at 0 °C in an ice-water bath. Then, the solution was stirred for 4 h at 0 °C after 4 ml 2-bromopropionyl bromide and 20 ml toluene were added dropwise over an hour, followed by stirring over night at room temperature. After the reaction completely, the final product was centrifuged (5000 rmp, 5 min) with a mixed solution of water/acetone for three times, and dried under vacuum for 24 h at 60 °C. The mixture with TiO_2–Br (2 g) and methanol (100 ml) was stirred for 30 min. 1.2 ml of PMDETA and 0.6 g CuBr were added into the mixture under the protection of nitrogen gas. Then, the ATRP reaction started after 5 ml of HEMA was injected into the flask for 12 h at 65 °C. The resultant mixture was purified with repeated centrifugal sedimentation (5000 rmp, 5 min) and clean solution of methanol and acetone for three times. TiO_2-HEMA was obtained after drying for 24 h at 60 °C.

2.3. Preparation of polymer separators

PI/PVdF-HFP and nanoparticles@PI/PVdF-HFP composite membranes were prepared by co-electrospinning process. The homogeneous PVdF-HFP solution (14 wt%) was prepared by dissolving the powder in a mixture solvent of DMF and acetone with the ratio of 7/3 (w/w) and nanoparticles@PI solutions (23 wt%) were obtained by dissolving the polymer and nanoparticles in NMP with magnetic stirring at the temperature of 70 °C for 10 h after 30 min ultrasonic treatment for dispersion liquid with various contents of nanoparticles (0, 1, 2, 3 wt% based on the weight of PI). Four-needle electrospinning apparatus was set up, two of which were fed with PVdF-HFP solution and others with nanoparticles@PI solution and the two types of polymer solutions were arrayed alternately, in a straight line to form a composite membrane, which could be referred to as co-electrospinning, followed by thermal calendering process to improve the mechanical property of the composite membranes via fusing PVdF-HFP having lower melting point. Then, the cells were assembled by using the resultant electrospun membranes as separators and Fig. 2 presented the preparation of f-T@PI/PH composite membrane and the cell assembly.

During electrospinning process, PVdF-HFP solution and nanoparticles@PI solution were drew with the same voltage of 20 kV and injected under the different flow rate of 1 ml h^{-1} and 1.5 ml h^{-1}, respectively. The distance between the needle (OD = 0.91 mm, ID = 0.61 mm) and the receiving drum (rotational speed of 2 RPM) was 20 cm. Needle plate embedded with four needles under 2 cm spacing moved reciprocally with the amplitude of 30 cm.

2.4. Characterization of nanoparticles and separators

The formation of covalent bonds of TiO_2 nanoparticles after ATRP reaction can be observed by Fourier transform infrared spectroscopy (FTIR) in the range of 400–4000 cm^{-1}. Ultraviolet–visible spectra recorded with a UV-1800 spectrophotometer have been used for comparing the dispersibility of TiO_2 nanoparticles before and after modification.

The morphologies of electrospun membranes were observed by field emission scanning electron microscopy (FESEM, S-4800) and the average fiber diameter was obtained by using ImagePro Plus software. Thickness of electrospun membranes was determined by CHY-C2 thickness tester. The mechanical properties of prepared electrospun membranes were measured by Instron 3369 universal

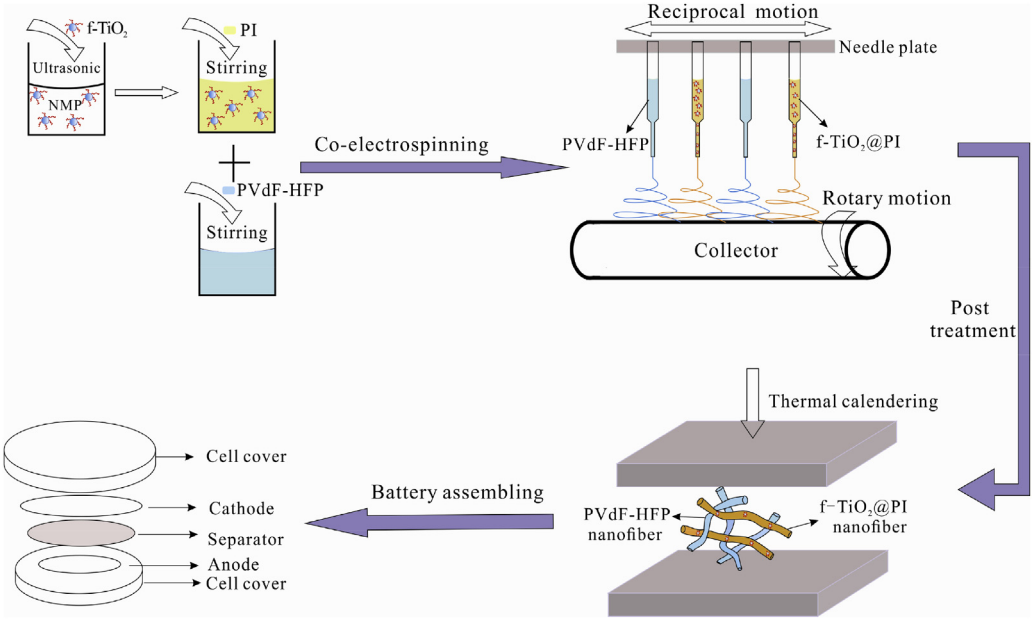

Fig. 2. The schematic illustration of the preparation of electrospun separator and battery assembling.

strength tester at a stretching speed of 10 mm s^{-1} with the sample straps of about 2 cm wide and 15 cm long. JC2000D1 contact angle device was used for measuring the liquid electrolyte contact angles of electrospun membranes. The porosity of separators was determined by immersing samples into n-butanol liquid for 2 h and calculated according to Equation (1):

$$\text{Porosity}(\%) = \frac{m_{\text{butanol}}/\rho_{\text{butanol}}}{(m_{\text{butanol}}/\rho_{\text{butanol}}) + m_{\text{sample}}/\rho_{\text{sample}}} \quad (1)$$

where m_{butanol} and m_{sample} are the weights of n-butanol incorporated separator and the dried separator, respectively. ρ_{butanol} and ρ_{sample} are the density of n-butanol and the dried separator, respectively.

To measure the electrolyte uptake, 1 M $LiPF_6$ in ethylene carbonate (EC)/diethyl carbonate (DEC) = 1/1 (v/v) was employed to soak separators for 2 h and the masses of separator before and after swelling in liquid electrolyte were measured to obtain the electrolyte uptake based on Equation (2):

$$\text{Uptake} = (W - W_0)/W_0 \times 100\% \quad (2)$$

where W_0 and W are the weights of separator before and after immersed in liquid electrolyte, respectively.

The thermal properties of the separators were measured by differential scanning calorimeter at a heating rate of 10 °C min^{-1} and visual comparison of thermal dimensional stability was conducted under the heat treatment temperature of 180 °C for 30 min.

The electrochemical stability window of the polymer electrolytes was determined by linear sweep voltammetry method conducted on a working electrode of stainless-steel electrode and a counter electrode of lithium metal over the potential range of 0–6 V at a scan rate of 10 mV s^{-1}. The electrochemical properties of polymer electrolytes were determined using CHI 660D electrochemical workstation. The bulk resistance and the interfacial resistance of liquid electrolyte-soaked separator were measured by AC impedance measurement evaluated by electrochemical impedance spectroscopy (EIS) over the frequency ranging from 0.1 Hz to 100 KHz with 5 mV of AC amplitude at room temperature, where stainless-steel plate electrodes and lithium metal electrodes were applied for bulk resistance and interfacial resistance measurement, respectively. The ionic conductivity was calculated by Equation (3):

$$\sigma = \frac{d}{RA} \quad (3)$$

where R is the bulk resistance of liquid electrolyte-soaked separator obtained from AC impedance measurement. d and A are the thickness and the area of the separator, respectively.

The electronic conductivity was measured by BDS50 Dielectric Spectrometer provided by Novocontrol GmbH. The cells (2032-type coin) were assembled by sandwiching the composite separator between metal lithium anode and $LiCoO_2$ cathode in a glovebox filled with dry argon. First-cycle charge–discharge test and cycling performance were performed between 2.8 V and 4.2 V at a current density of 0.5C with a battery test system provided by Wuhan LISUN co., Ltd, China.

3. Results and discussions

3.1. Characterization of nanoparticles

The FTIR was used for confirming the successful preparation of f-TiO_2 nanoparticles and Fig. 3 presented the FTIR spectra of TiO_2 and f-TiO_2 nanoparticles. It can be seen from the spectrum of pristine TiO_2 that the characteristic absorption peak below 900 cm^{-1} signified the stretching vibration of Ti–O–Ti and the broad absorption peak around 3425 cm^{-1} corresponded to the stretching vibration of hydroxyl groups on nanoparticle surface. As for the spectrum of f-TiO_2, the absorption peak 3425 cm^{-1} became broader, which is attributed to the hydroxyl group on HEMA [19,20]. Moreover, compared with pure TiO_2, there appeared several new absorption peaks. The peaks at 2925 cm^{-1} and 953 cm^{-1} are assigned to the stretching vibration of C–H bonds. The stretching vibration of 1720 cm^{-1} is ascribed to the C=O correlated with HEMA units. In addition, the absorption peak at 1253 cm^{-1} is corresponding to the stretching vibration of C–O bond [19]. These indicated that HEMA was grafted onto TiO_2 nanoparticle successfully.

UV–vis absorption spectra have been used for characterization of the dispersion stability of nanoparticles in previous studies [21,22]. Absorbance at the characteristic peak represents a measure of the relative turbidity of the samples and it will decrease on account of the clarification of the base fluid as the sedimentation occurs [23], suggesting the dispersion instability of suspension [24]. Fig. 4 shows the UV–vis absorption spectra of TiO_2 and f-TiO_2 nanoparticles dissolved in NMP solvent. It can be seen that the

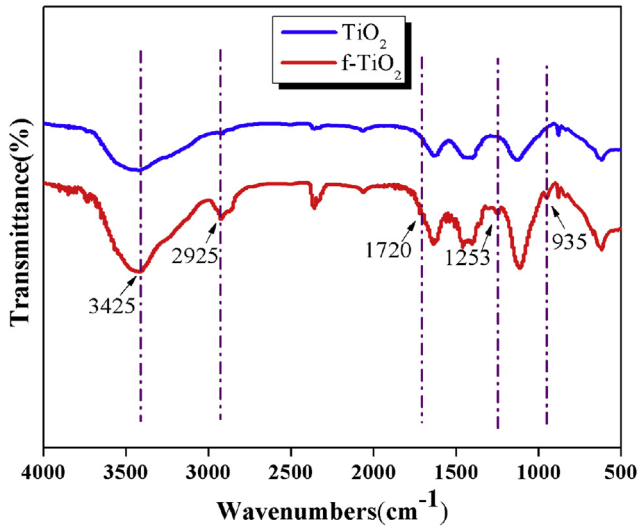

Fig. 3. The FTIR spectra of TiO_2 and f-TiO_2 nanoparticles.

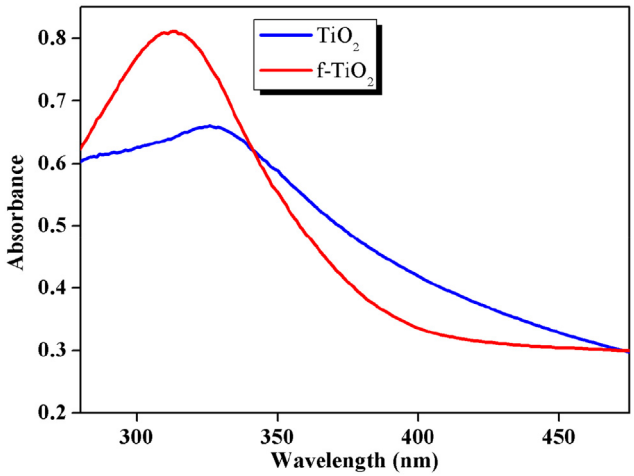

Fig. 4. UV–vis absorption spectrum of TiO_2 and f-TiO_2 nanoparticles in NMP.

absorbance of f-TiO_2 nanoparticle is higher than that of TiO_2, which indicated that f-TiO_2 nanoparticle dispersed in NMP steadily and homogeneously. Excellent dispersion stability can play a positive role in improving the physical properties of electrospun membranes, as discussed below.

3.2. Preparation and characterization of electrospun composite membrane

Fig. 5 showed the SEM images of composite membranes and PI diameter distributions with various nanoparticle concentrations (0%, 1%, 2% and 3%). It can be seen that pure PI fiber has an average diameter of 1222 nm and it decreased to 931 nm and 856 nm with the addition of 1% and 2% TiO_2 nanoparticle. Similarly, the average diameter of PI fiber with 1% and 2% f-TiO_2 nanoparticle decreases to 750 nm and 689 nm. It is attributed that the repulsive force of nanoparticle minimizes entanglement of polymer chains [18,25]. Moreover, the incorporation of f-TiO_2 nanoparticle further decreases the average fiber diameter compared with the TiO_2@PI fiber, which could be explained by the fact that f-TiO_2 dispersed more homogeneously [17]. However, beaded fibers with larger average fiber diameter were produced when nanoparticle concentration amounted to 3% and it is resulted from the agglomeration of nanoparticles [17].

The presence of nanoparticle within the fiber is investigated by Energy Dispersive Spectroscopy (EDS) and the EDX spectra of 2% T@PI/PH and 2% f-T@PI/PH membranes were shown in Fig. 5D and E. It was observed that the characteristic peak of Ti element occurred at 4.5 keV for both two kinds of composite membranes. It has been seen from Fig. 5E that the characteristic Si peak appeared at 1.8 keV for the 2% f-T@PI/PH due to the addition of 3-aminopropyl triethoxysilane during the atom transfer radical polymerization. Additionally, compared with T@PI/PH membrane, the content of C and O element slightly increased for f-T@PI/PH membrane demonstrated by higher intensity in EDX spectrum, which indicated the presence of HEMA.

Fig. 6(a) presents the porosity of composite electrospun membranes with various contents of nanoparticles after the thermal calendering process with the temperature of 135 °C, pressure of 0.8 MPa and calendering time of 5 min. It was observed that the porosity of composite membranes increased by the addition of lower amount of nanoparticles and then decreased by the more incorporation of nanoparticles. It is well known that the porosity is strongly dependent on the fiber diameter [17,18,26]. Therefore, f-T@PI fiber could form more void space due to much smaller fiber diameter than that of pure PI and T@PI fibers, which resulted in higher porosity of f-T@PI/PH composite membranes. Nevertheless, beaded PI fiber with relatively larger diameter leads to declined porosity when the concentration of nanoparticles amounted to 3%.

The liquid electrolyte uptake behavior of thermal calendered electrospun membranes with different amounts of TiO_2 and f-TiO_2 was also showed in Fig. 6(a). The liquid electrolyte uptake of membranes increased and then decreased whether adding TiO_2 or f-TiO_2 nanoparticles. As for T@PI/PH membranes, apart from the interconnected structure which was beneficial to absorb more liquid electrolyte, the addition of TiO_2 nanoparticle possessing the polar group of O—H further enhanced the liquid electrolyte uptake. Thus, the electrolyte uptake of nascent PI/PH membrane was lower than that of T@PI/PH. It also can be seen from Fig. 6(a) that the electrolyte uptake of f-T@PI/PH membranes was higher than that of

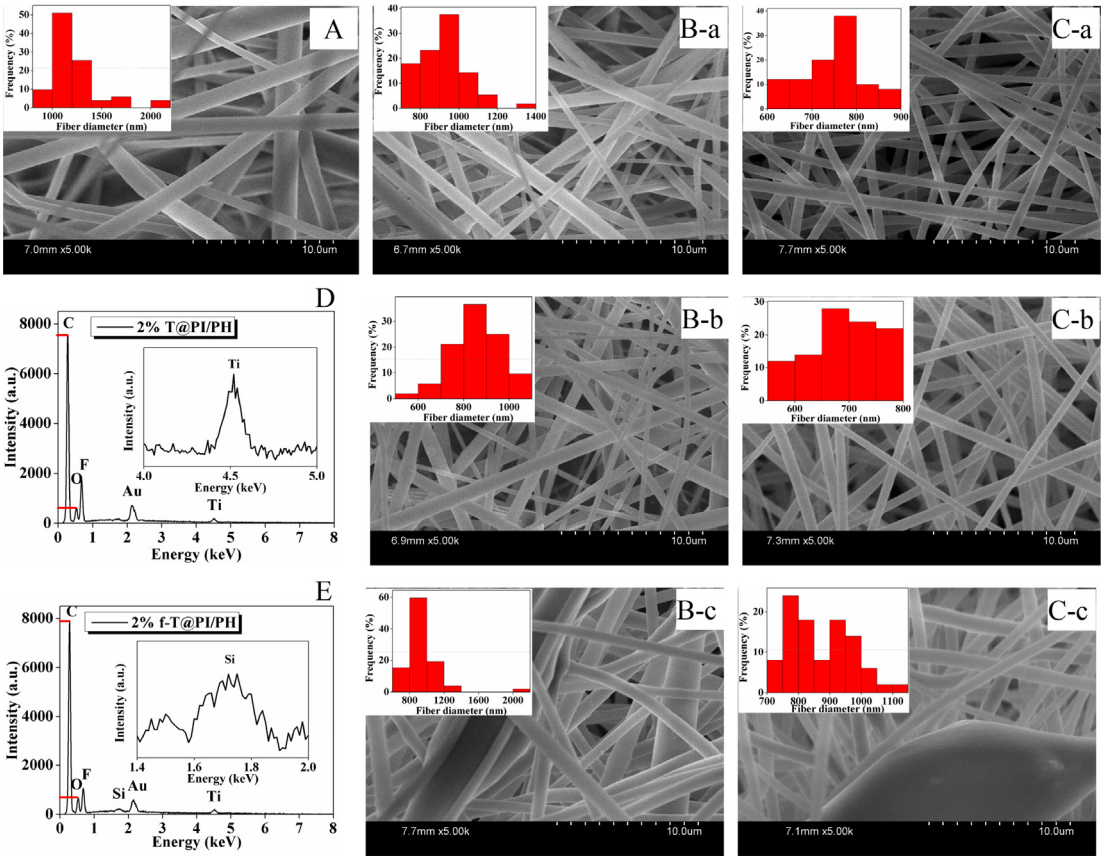

Fig. 5. The SEM images of (A) PI/PH, (B) T@PI/PH and (C) f-T@PI/PH with different nanoparticle concentration of (a) 1%, (b) 2% and (c) 3% and EDS spectra of (D) 2% T@PI/PH and (E) 2%.f-T@PI/PH.

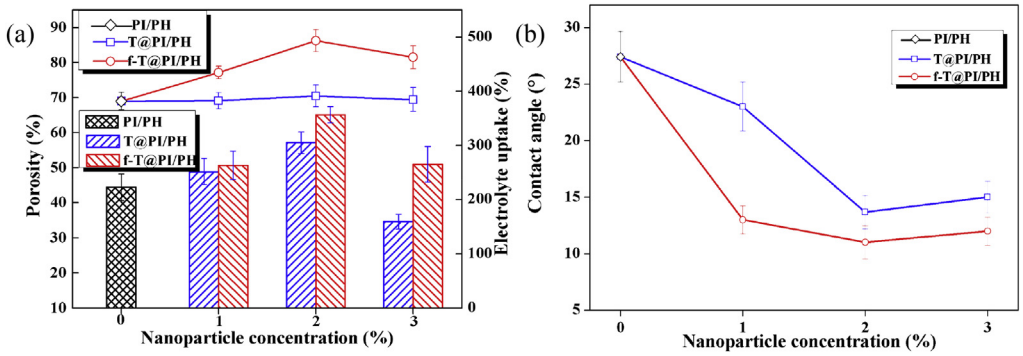

Fig. 6. (a) Porosity, liquid electrolyte uptake and (b) liquid electrolyte contact angle of electropsun composite membranes with different nanoparticle concentration (0%, 1%, 2% and 3%) after thermal calendering process.

T@PI/PH membranes. The reasons can be explained as follows: (I) the porous structure of f-T@PI/PH membranes with higher porosity can take in much more liquid electrolyte. (II) f-TiO_2 nanoparticles served to excellent affinity between carbonate-based liquid electrolyte and the membrane due to the abundant hydroxyl groups in HEMA grafted on TiO_2. (III) The aggregation of TiO_2 nanoparticle declined the effective surface and then hindered the function of TiO_2 nanoparticle, which resulted in lower liquid electrolyte uptake.

Contact angle measurement was used to evaluate the liquid electrolyte wettability of composite electrospun membranes. The contact angles of electrospun membranes after thermal calendering treatment with different concentration of TiO_2 and f-TiO_2 nanoparticles were illustrated in Fig. 6(b). It is observed that the contact angle of nascent PI/PH membrane is about 27.4° and with the increase of nanoparticle concentration, the contact angle decreased although a slight rise occurred at the concentration of 3%, suggesting improved wettability of membranes. It could be ascribed to the addition of nanoparticles covered with plentiful hydroxyl groups and Ti—O bonds. In addition, abundant of oxygen-containing groups f-T@PI/PH membrane possessed resulted in lower contact angles than that of T@PI/PH membranes.

3.3. Mechanical and thermal properties of electrospun composite membrane

3.3.1. Mechanical property of electrospun composite membrane

Stress-strain curves of various electrospun composite membranes were measured to evaluate the mechanical property of the samples with TiO_2 and f-TiO_2 nanoparticles, as shown in Fig. 7(d). Before the thermal calendering process, the slight decrease of tensile strength of 2%T@PI/PH membrane may be attributed to the bad interfacial interaction between nanoparticle and polymer matrix [27]. However, on the basis of coupling agents, living radical polymerization can modify the surface of the TiO_2 nanoparticles

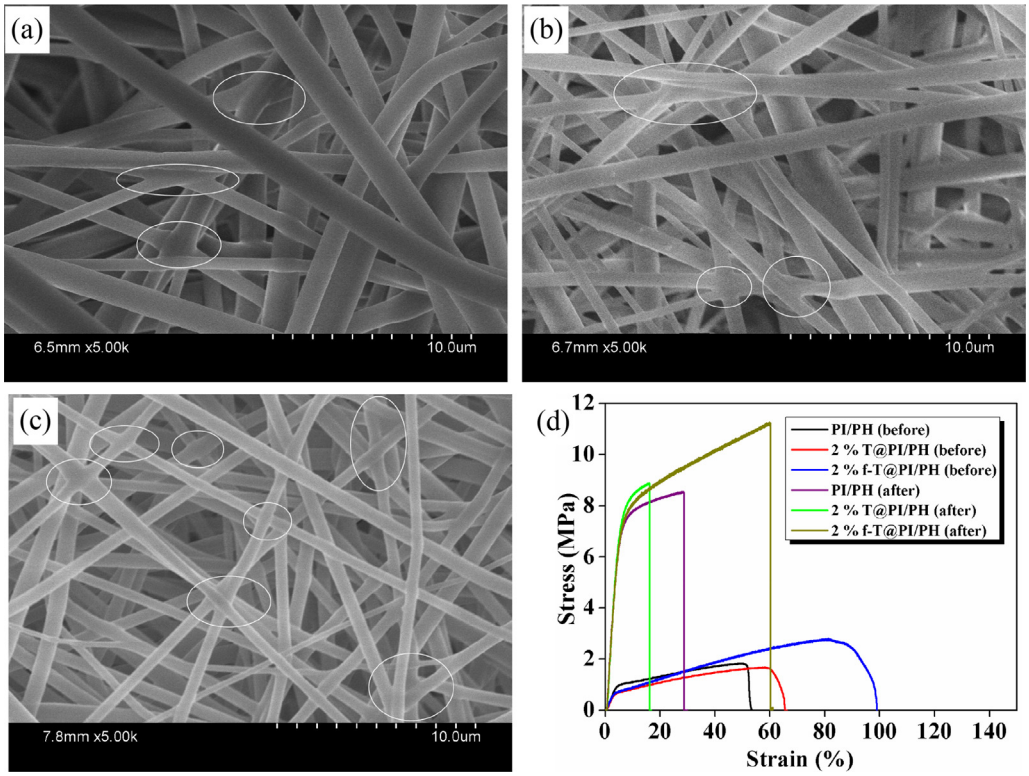

Fig. 7. The morphologies of (a) PI/PH, (b) 2% T@PI/PH, (c) 2% f-T@PI/PH membranes after thermal calendering process and (d) the stress–strain curves before and after thermal calendering process of membranes.

and then covalent attachment to polymer chains can minimize agglomeration and strengthen the interaction between nanoparticles and polymer matrix. Therefore, the tensile strength of 2% f-T@PI/PH membrane is higher than that of 2% T@PI/PH and PI/PH membranes. It can be also seen that the tensile strengths of membranes were all improved by more than three times after the thermal calendering process, which was attributed to the several bonded points appearing between two fibers or more (cf. Fig. 7(a)–(c)) caused by the fusion of PVdF-HFP component with lower melting temperature. And the tensile strength of 2% f-T@PI/PH membrane is higher than that of 2% T@PI/PH and PI/PH membranes. This phenomenon could be explained as follows: The decrease of PI fiber diameter increases the contact surface area between two PVdF-HFP fibers or more, which served to form more bonded points (cf. Fig. 7(c)) beneficial for further improving the mechanical property of electrospun membranes.

3.3.2. Thermal property of electrospun composite membrane

Thermal stability of separators is also an important indicator to guarantee the battery safety performance [8,28]. The DSC curves and photographs of thermal dimensional stability were presented in Fig. 8. It is observed from Fig. 8(a) that an endothermic peak occurred at about 135 °C which represents the melting temperature of the PVdF-HFP component. Additionally, another small endothermic peak appeared at about 220 °C corresponding to the glass transition temperature of the PI component. Furthermore, the electrospun composite membranes exhibited excellent thermal dimensional stability without dimensional change whether nanoparticles were added or not. As for the nascent PI/PH composite membrane, heat resistant PI served as the skeleton to maintain the integrity of separators. Moreover, apart from the function of PI component, inorganic nanoparticles in modified composite membranes also acted as the role of heat resistant materials to guarantee the thermal dimensional stability.

3.4. Electrochemical performances of composite separator

The ionic conductivities of the composite separators were determined by AC impedance spectroscopy measurements performed on symmetric two stainless steel electrode cells and the intercept of the impedance spectrum at the real axis represented the bulk resistance of the electrolyte solution in the pores of the separator [29]. It is observed from Fig. 9 that the bulk resistance of the polymer electrolytes follows the order PI/PH (1.2 Ω) > 2% T@PI/PH (0.9 Ω) > 2% f-T@PI/PH (0.6 Ω) and correspondingly, the ionic conductivities are 1.18 mS cm^{-1}, 1.57 mS cm^{-1} and 2.36 mS cm^{-1}, respectively. The larger ionic conductivities of fibrous polymer electrolytes with TiO_2 and f-TiO_2 nanoparticles can be mainly ascribed to higher liquid electrolyte uptake and better liquid electrolyte wettability (cf. Fig. 6(a) and (b)) which contributed to the formation of more channels allowing greater lithium ions to migrate the polymer electrolyte. Furthermore, the excellent affinity between HEMA and carbonate-based liquid electrolyte and polar surface groups of nanoparticles introducing Lewis acid/based interactions with the ionic species in the liquid electrolyte also made contribution to the improved ionic conductivities of modified fibrous polymer electrolytes [30].

Fig. 10 shows the electrochemical impedance spectroscopy (EIS) of the symmetric Li^+/Li cells with different electrospun composite separators. The large semicircle at high frequency range corresponds to the impedance of surface film formed on the lithium electrode and the small semicircle at medium-to-low frequency region represents the impedance of charge transfer and ionic diffusion through interface [31]. It can be seen from Fig. 10 that ignorable semicircle of three kinds of cells with fibrous separator at medium-to-low frequency revealed that charge transfer impedance could be neglected. Besides, the cells assembled with T@PI/PH and f-T@PI/PH membranes possessed lower interfacial impedance at high frequency range than that of nascent PI/PH separator, which indicated that lithium ions easily immigrated through the surface film on the electrode. It is ascribed to the higher porosity, electrolyte uptake and better electrolyte wettability. Furthermore, the interfacial impedance of the cell with f-T@PI/PH separator is slightly smaller than that of the cell with T@PI/PH and it could be explained by the excellent affinity between HEMA and carbonate-based liquid electrolyte.

The electrochemical stability was determined by linear sweep voltammetry (LSV) performed on the Li/separator/SS system cells at a scan rate of 10 mV s^{-1} ranging from 0 to 6 V and the electrochemical oxidation limit was decided by the formation of sharp increased current when the electrolyte decomposed. Generally, the working potential of practical lithium-ion rechargeable batteries was ranging from 1.8 V to 3.5 V versus Li^+/Li [10,18]. As shown in Fig. 11, there were no apparent increases in anodic currents below 4.5 V for all separators, which indicated that those electrospun separators are compatible with the carbonate electrolyte and have sufficient electrochemical stability to be charged and discharged against the anodic potential applied in this work (4.2 V). Furthermore, T@PI/PH and f-T@PI/PH separators exhibited slightly higher decomposition voltage, which demonstrated that the modified fibrous separators possessed better electrochemical stability. Apart from the much more liquid electrolyte entrapped in the pores of fibrous separators resulted from good swelling ability originated from higher porosity, thinner fiber diameter and morphology with

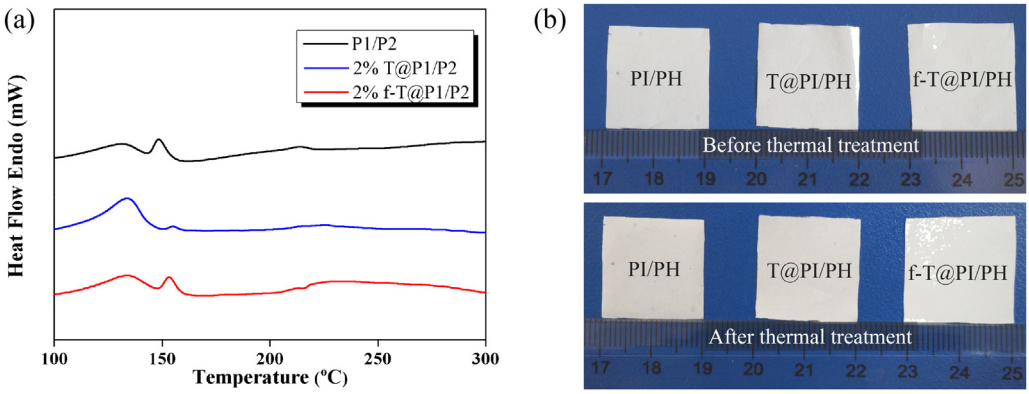

Fig. 8. (a) DSC curves of PI/PH, 2% T@PI/PH and 2% f-T@PI/PH after thermal calendering process and (b) photograph of composite electrospun membranes before and after thermal treatment.

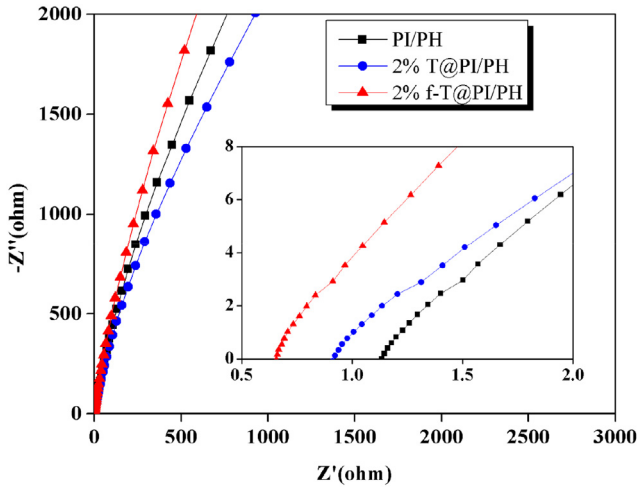

Fig. 9. Nyquist plots of SS/electrolyte-soaked separator/SS cells at room temperature.

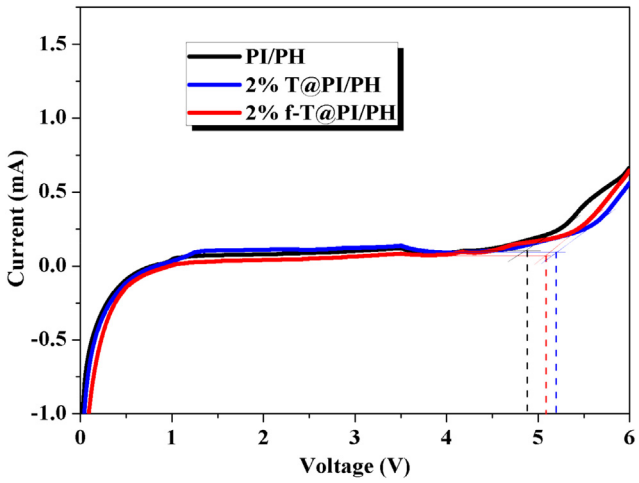

Fig. 11. Linear sweep voltammograms of different electrospun separators.

multi-porous structure [17], Lewis acid/based interactions with the ionic species in the liquid electrolyte can reduce the decomposition of the lithium salt anion, which also served to higher electrochemical potential window [32].

3.5. Battery performances

Before characterizing the battery performances, the electronic conductivities of electrospun membranes were evaluated by BDS50 Dielectric Spectrometer to further confirm whether the prepared electrospun membranes can be used for separators. The electronic conductivities under the frequency of 0.01 Hz of PI/PH, 2%T@PI/PH, 2%f-T@PI/PH membranes and Celgard 2400 separator as comparison were 2.91×10^{-15} S cm^{-1}, 2.31×10^{-13} S cm^{-1}, 1.88×10^{-13} S cm^{-1} and 4.95×10^{-13} S cm^{-1}, respectively. Although the electronic conductivities of 2%T@PI/PH and 2%f-T@PI/PH membranes were higher than that of PI/PH membrane, they are still lower than that of Celgard 2400 separator. Thus, the electrospun membranes can be used as battery separators without potential safety hazard.

The coin-type cells were fabricated with $LiCoO_2$ as cathode and metal lithium as anode in order to evaluate the feasibility of rechargeable lithium ion batteries with PI/PH and nanoparticle@PI/PH membrane as separators. The first-cycle charge–discharge profiles of Li/$LiCoO_2$ cells assembled with PI/PH, 2%T@PI/PH and 2% f-T@PI/PH membranes and cycled under a voltage range of 2.8–4.2 V at current density of 0.5C were presented in Fig. 12. It is seen that the first-cycle discharge capacity of the Li/$LiCoO_2$ cell is 159 mAh g^{-1} when pristine PI/PH membrane served as battery separator. For the cells with 2%T@PI/PH and 2%f-T@PI/PH fibrous separators, the first-cycle discharge capacities were 165 mAh g^{-1} and 170 mAh g^{-1}, respectively. Nanoparticle@PI/PH membranes have higher porosity and liquid electrolyte uptake than those of pristine PI/PH membrane, and as a result, they possess larger ionic conductivities and can offer more conduction channels, which facilitated the repeated intercalation/de-intercalation of lithium ion in/from the electrode materials, leading to increased discharge capacities [33]. Similarly, the difference in initial discharge between the cells assembled with 2%T@PI/PH and 2%f-T@PI/PH membrane is due to the larger ionic conductivity discussed in Sec. 3.4.

Fig. 13 shows the cycling performance of Li/$LiCoO_2$ cells at 0.5C. For the cell assembled with PI/PH fibrous separator, apparent

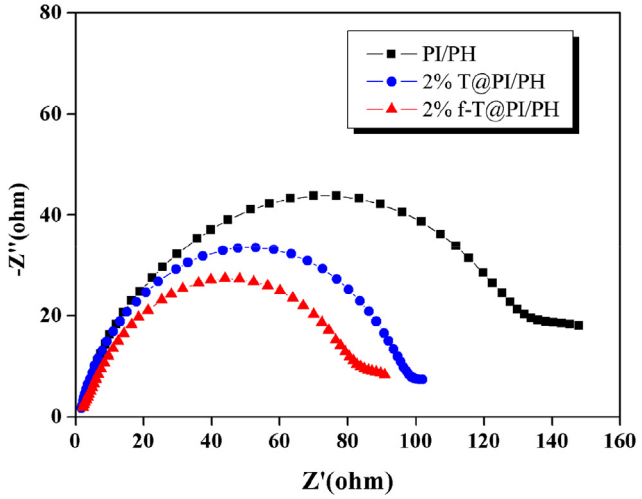

Fig. 10. The AC impedance spectra of the half-cell with different electrospun separators.

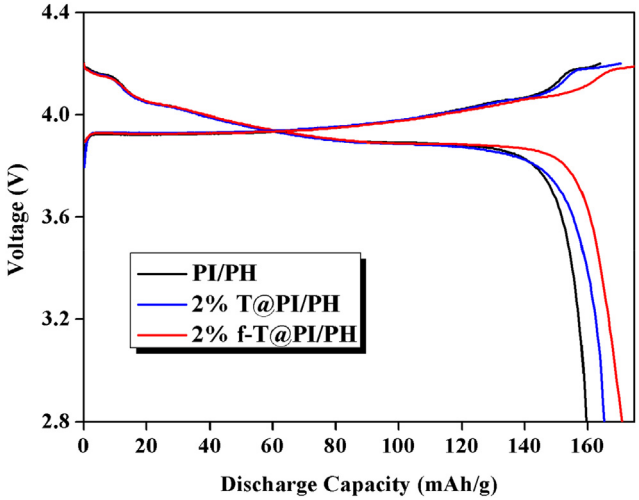

Fig. 12. First-cycle charge–discharge curves of Li/$LiCoO_2$ cells containing PI/PH, 2% T@PI/PH and 2%f-T@PI/PH fibrous separator at 0.5C.

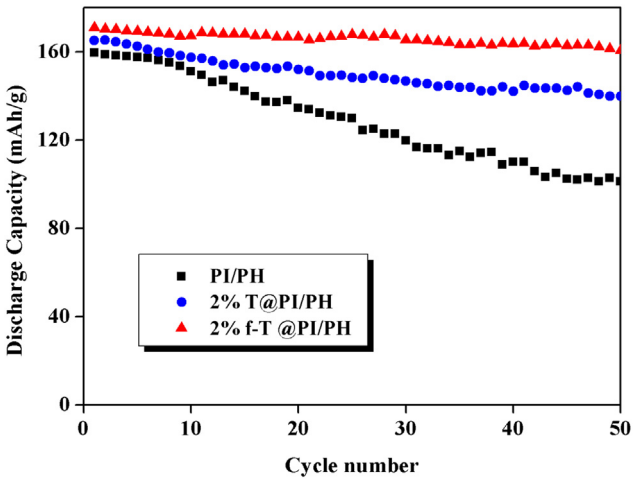

Fig. 13. Cycling performance of Li/$LiCoO_2$ cells containing PI/PH, 2%T@PI/PH and 2%f-T@PI/PH fibrous separator at 0.5C.

capacity loss can be observed and the discharge capacity after 50 cycles declined to 101 mAh g^{-1} with lower capacity retention of 64%. In addition, the discharge capacity of the cell with 2%T@PI/PH separator reduced to 140 mAh g^{-1} and the capacity retention is 85% after 50 cycles. The improvement in cycling performance is in agreement with the increased of liquid electrolyte uptake and ionic conductivity because these factors endow easier ion transport and better electrolyte retention during cycling [34]. Compared with previous two kinds of cells, no significant capacity loss is observed for the cell with 2%f-T@PI/PH fibrous separator and the discharge capacity reached to 161 mAh g^{-1} with the capacity retention of 95% after 50 cycles. Based on previous investigations in Sec. 3.2 and 3.4, 2%f-T@PI/PH membrane has highest electrolyte uptake and ionic conductivity due to higher porosity and excellent affinity between carbonate-based and liquid electrolyte. Therefore, 2%f-T@PI/PH separator can effectively retain more liquid electrolyte and better cycle performance can be obtained for the corresponding battery.

4. Conclusions

The composite nanoparticles@PI/PH membranes used for battery separators were prepared by co-electrospinning process. f-TiO_2 nanoparticle with better dispersibility produced by ATRP method reduced the PI fiber diameter and then improved the physical property of electrospun membranes including porosity, liquid electrolyte uptake and wettability. Furthermore, excellent mechanical property and thermal dimensional stability of membranes endow the battery with higher safety performance. Superior ionic conductivity, interfacial and electrochemical stability as well as excellent cycling performance also demonstrated that co-electrospun 2% f-TiO_2@PI/PH membranes were suitable for lithium ion battery separator. Overall, it can be concluded that minimizing the stacking effect and aggregation of inorganic nanoparticles and maintaining their own raw property of polymers are effective ways to improve the performances of electrospun membrane, especially served as lithium ion battery separator.

Acknowledgment

This work was supported by National Science Foundation of China, with the project approval No. of 51373121 and by a grant from Tianjin Municipal Science and Technology Commission under Contract No. 10JCYBJC03300.

References

[1] P.B. Balbuena, Y. Wang, Lithium-ion Batteries, World Scientific, 2004.
[2] G.-A. Nazri, G. Pistoia, Lithium Batteries: Science and Technology, Springer Science & Business, 2008.
[3] G. Venugopal, J. Moore, J. Howard, S. Pendalwar, J. Power Sources 77 (1999) 34–41.
[4] D. Linden, T.B. Reddy, in, McGraw-Hill Companies, Inc., 1865.
[5] S.S. Zhang, J. Power Sources 164 (2007) 351–364.
[6] W.-K. Shin, D.-W. Kim, J. Power Sources 226 (2013) 54–60.
[7] W. Jiang, Z. Liu, Q. Kong, J. Yao, C. Zhang, P. Han, G. Cui, Solid State Ionics 232 (2013) 44–48.
[8] J. Zhang, Z. Liu, Q. Kong, C. Zhang, S. Pang, L. Yue, X. Wang, J. Yao, G. Cui, Acs Appl. Mater. Interfaces 5 (2013) 128–134.
[9] C. Chengying, T. Lei, L. Weiwei, M. Jiquan, L. Lei, J. Power Sources 248 (2014) 224–229.
[10] M. Yanilmaz, Y. Lu, M. Dirican, K. Fu, X. Zhang, J. Membr. Sci. 456 (2014) 57–65.
[11] N. Kimura, T. Sakumoto, Y. Mori, K. Wei, B.-S. Kim, K.-H. Song, I.-S. Kim, Compos. Sci. Technol. 92 (2014) 120–125.
[12] N. Wu, Q. Cao, X. Wang, S. Li, X. Li, H. Deng, J. Power Sources 196 (2011) 9751–9756.
[13] L. Juneun, L. Cho-Long, P. Kyusung, K. Il-Doo, J. Power Sources 248 (2014) 1211–1217.
[14] B. Hojjati, R. Sui, P.A. Charpentier, Polymer 48 (2007) 5850–5858.
[15] S. Haque, I. Rehman, J.A. Darr, Langmuir 23 (2007) 6671–6676.
[16] W. Chen, Y. Liu, Y. Ma, J. Liu, X. Liu, Mater. Lett. 133 (2014) 67–70.
[17] H.-R. Jung, D.-H. Ju, W.-J. Lee, X. Zhang, R. Kotek, Electrochim. Acta 54 (2009) 3630–3637.
[18] M. Yanilmaz, C. Chen, X. Zhang, J. Polym. Sci. Pol. Phys. 51 (2013) 1719–1726.
[19] J.T. Park, J.H. Koh, J.A. Seo, J.H. Kim, J. Mater. Chem. 21 (2011) 17872–17880.
[20] G. Zhang, S. Lu, L. Zhang, Q. Meng, C. Shen, J. Zhang, J. Membr. Sci. 436 (2013) 163–173.
[21] S. Zhou, L. Wu, M. Xiong, Q. He, G. Chen, J. Dispers. Sci. Technol. 25 (2005) 417–433.
[22] W.T. Cheng, C.W. Hsu, Y.W. Chih, J. Colloid Interface Sci. 270 (2004) 106–112.
[23] M.C.C.D. Ignacio, E.K. Peralta, M.M. Peralta, A.R. Elepaño, D.C. Suministrado, Philipp. J. Crop Sci. 39 (2014) 20–29.
[24] M. Licchelli, M. Malagodi, M. Weththimuni, C. Zanchi, Appl. Phys. A 114 (2014) 673–683.
[25] L. Ji, X. Zhang, Mater. Lett. 62 (2008) 2161–2164.
[26] L. Zhou, N. Wu, Q. Cao, B. Jing, X. Wang, Q. Wang, H. Kuang, Solid State Ionics 249 (2013) 93–97.
[27] H. Yang, F. Li, C. Shan, D. Han, Q. Zhang, L. Niu, A. Ivaska, J. Mater. Chem. 19 (2009) 4632–4638.
[28] Y.-E. Miao, G.-N. Zhu, H. Hou, Y.-Y. Xia, T. Liu, J. Power Sources 226 (2013) 82–86.
[29] L.C. Zhang, X. Sun, Z. Hu, C.C. Yuan, C.H. Chen, J. Power Sources 204 (2012) 149–154.
[30] W.-W. Cui, D.-Y. Tang, Z.-L. Gong, J. Power Sources 223 (2013) 206–213.
[31] X. Huang, J. Power Sources 256 (2014) 96–101.
[32] M. Deka, A. Kumar, J. Power Sources 196 (2011) 1358–1364.
[33] H.-S. Jeong, S.-Y. Lee, J. Power Sources 196 (2011) 6716–6722.
[34] F. Croce, M.L. Focarete, J. Hassoun, I. Meschini, B. Scrosati, Energy Environ. Sci. 4 (2011) 921–927.